Minimizing oxygen permeability in chitin/cellulose nanomaterial coatings by tuning chitin deacetylation

Yue Ji[1], Samantha Waters[1], Eunhyang Lim[1], Augustus W. Lang[2,3], Peter N. Ciesielski[4], Meisha L. Shofner[2,3], John R. Reynolds[3,5,6], J. Carson Meredith[1,2]*

[1] School of Chemical & Biomolecular Engineering, Georgia Institute of Technology, Atlanta, GA 30332, USA

[2] Renewable Bioproducts Institute, Georgia Institute of Technology, Atlanta, GA 30332, USA

[3] School of Materials Science and Engineering, Georgia Institute of Technology, Atlanta, GA 30332, USA

[4] Renewable Resources and Enabling Sciences Center, National Renewable Energy Laboratory, Golden, CO 80401, USA

[5] School of Chemistry and Biochemistry, Georgia Institute of Technology, Atlanta, GA 30332, USA

[6] Center for Organic Photonics and Electronics, Georgia Tech Polymer Network, Georgia Institute of Technology, Atlanta, GA 30332, USA

*Corresponding author: carson.meredith@chbe.gatech.edu

ABSTRACT: The demand for packaging materials with low gas permeabilities is increasing, but commonly used petroleum-derived single-use plastics are not renewable, biodegradable, or easy to recycle. Nanomaterials composed of chitin and cellulose, which are abundant in nature, have high crystallinities and low oxygen permeabilities (OP), providing a viable alternative. In this work, we explore how deacetylation conditions of crab shell chitin can be used to tune the charge and size of resulting chitin nanowhiskers (ChNWs) and the resulting OP of layered film structures. Three deacetylation factors, the concentration of sodium hydroxide (%NaOH), temperature (T), and reaction time, were explored using a three-factor three-level Taguchi design with an orthogonal array. The resulting ChNW suspensions were sequentially spray-coated with suspensions of cellulose nanocrystals (CNCs) onto cellulose acetate (CA) films to form a multilayer structure. We show that ChNWs prepared under more aggressive deacetylation conditions inside the original orthogonal array (higher %NaOH, T, and time) had shorter lengths but the surface charge was significantly influenced only by more aggressive deacetylation outside of the original design conditions. With only ~10% decrease in the ultimate tensile strength and no significant loss in failure strain, the ChNW-CNC coating resulted in ~20% decrease in WVTR in comparison to uncoated CA films. The optimization of process conditions resulted in CA-ChNW-CNC films with a 91-99% decrease in OP (132-16.7 $cm^3 \cdot \mu m/m^2/day/kPa$ versus 1553 $cm^3 \cdot \mu m/m^2/day/kPa$ for uncoated CA).

KEYWORDS: Chitin nanowhiskers, cellulose nanocrystals, multilayer coating, oxygen permeability, Taguchi method

INTRODUCTION

Packaging is necessary for maintaining the quality, safety, and integrity of food, beverages, pharmaceuticals, and consumer electronic products.[1-4] Food packaging should hinder the gain or loss of water vapor and oxygen, which contribute significantly to the deterioration of food.[5] Thus, a high barrier against water vapor and oxygen is an important performance property of food packaging materials. Currently, the most widely used materials in food packaging are petroleum-based plastics,[6,7] including polyolefins, poly(vinyl chloride), poly(vinylidene chloride) (PVDC), nylon, poly(ethylene-co-vinyl alcohol), and poly(ethylene terephthalate) (PET). These are non-renewable and degrade over hundreds of years in typical landfill conditions.[8] As a result, plastic packaging contributes to 750 million pieces, 22 million tons, of plastic that go to landfill or the environment annually.[9] Because polysaccharides degrade via microbial routes, these materials present opportunities for reducing landfill utilization and environmental accumulation of plastics.

Cellulose[10] and chitin,[11] the most abundant polysaccharides, have attracted significant attention recently as potential components of sustainable materials. Cellulose is a homopolymer of glucose, while chitin is a homopolymer of N-acetyl glucosamine. Due to strong inter- and intra-chain hydrogen bonding, these polymers tend to form macromolecular assemblies that are highly crystalline, which leads to high strength and gas barrier properties.[12,13] For instance, it has been found that films formed from chitin nanofibers (ChNFs),[14] chitin nanowhiskers (ChNWs),[15] cellulose nanofibrils (CNFs),[16] and cellulose nanocrystals (CNCs)[17,18] have low oxygen permeability (OP), i.e., lower than 4 $cm^3 \cdot \mu m/m^2/day/kPa$.[19] Previous work showed that multilayer coatings containing alternating nanocellulose (anionic) and nanochitin (cationic) take advantage of their electrostatic attraction and promote densification at the interface.[20-23] For example, sprayed

multilayer coatings on poly(lactic acid) (PLA) substrates had OP values that were 65% lower than the single-layer coatings of CNC or ChNF.[22]

Cellulose is mainly sourced from plants, while chitin is found in the exoskeleton of arthropods or the cell walls of fungi or yeast. The most common current industrial sources of chitin are crab and shrimp shells that are waste byproducts from food processing.[24] Crab shells have a hierarchical structure, and chitin is assembled with proteins and embedded in calcite;[25] thus, the extraction of chitin from crab shells usually involves deproteination in an alkaline solution and demineralization in an acidic solution. A deacetylation step is sometimes utilized to partially remove acetyl groups, depending on the charge desired on the final product. The resulting chitin with a lower degree of acetylation (DA) is more highly charged (in acid media) due to protonation of the primary amine groups and is more water-soluble, resulting in wider applications of the chitin.[26]

Because the size and charge of the ChNWs will affect the assembly of dense barrier structures, as well as interactions with anionic CNCs, it is reasonable to expect that the OP of the multilayer coating can be adjusted by tuning the properties of ChNWs. In most reports detailing the preparation or the applications of chitin, researchers applied either highly acetylated chitin (DA > 85%)[27,28] or highly deacetylated chitosan (DA < 15%),[29,30] where chitosan with a 0 % DA is a glucosamine homopolymer. The literature about the optimization of the purification process has focused on obtaining chitin with a high DA and molecular weight to reduce chitin degradation[31,32] or on producing chitosan with a low DA for better aqueous solubility.[33] Nevertheless, there remain limited studies on the influence of the deacetylation conditions on the barrier properties of the final product, particularly for intermediate DA. The deacetylation process is usually carried out in concentrated NaOH solution (40%-50%)[34] at a high temperature (>

80°C).[35] In contrast to deproteination at lower NaOH concentrations (< 17%),[36] using concentrated NaOH solution at higher reaction temperatures for longer reaction times also decreases the DA chitosan.[37] We propose that the properties of ChNWs can be tuned by a multivariable optimization of these deacetylation conditions, in order to minimize gas permeability in both ChNW single layer coatings as well as ChNW-CNC bilayers.

In this work, the OP of cellulose acetate (CA) films coated with sequential layers of ChNWs and CNCs to form a bilayer was optimized by exploring the influence of the ChNW deacetylation conditions. CA, a cellulose derivative widely available as a film, but with a high OP, was selected as a renewable substrate. The Taguchi design of experiment method[38] was employed to study the effects of chitin deacetylation on the OP of CA films coated with a ChNW-CNC bilayer. Three variables in the deacetylation step were studied by using a multivariable optimization to tune the preparation of chitin: the concentration of NaOH, the temperature, and the reaction time. The chitin was homogenized into a suspension that was characterized in terms of viscosity and ChNW dimensions and DA. The barrier properties (oxygen and water vapor) and mechanical properties of spray-coated films produced from the suspensions were also characterized. The optimal deacetylation conditions and the effect of each factor were determined statistically based on the OP of the coated CA.

EXPERIMENTAL METHODS

Materials

Crab shell flakes (Neptune's Harvest, USA), sodium hydroxide (NaOH; ACS grade, VWR, USA), hydrochloric acid (HCl; ACS grade, Sigma-Aldrich, USA), acetic acid (HOAc; Sigma-Aldrich, USA), and a 10 wt% cellulose nanocrystal suspension (CNC; USDA Forest Products Laboratory, USA) with 1.06 wt% sulfur content on dried CNC which was extracted from black

spruce (*Picea mariana*) and diluted to 0.5 wt% for this study were all used without further purification. The cellulose acetate (CA) substrates were purchased from Goodfellow Cambridge Ltd., USA, and the properties are available in Table S1.

Extraction of chitin

Chitin was extracted from crab shells with the methods similar to those previously reported.[14,22] Crab shells were treated first with 5 wt% NaOH and refluxed with an oil bath at 140℃ for 6 hours to remove the proteins. Then, they were treated with 7 wt% HCl at room temperature for 6 hours for demineralization. The pre-purified chitin was deacetylated with a baseline typical treatment utilizing 25 mL of 35 wt% NaOH solution per gram of chitin, heated with an oil bath at 140℃ for 100 min.[15,39] After each step, the chitin was washed with tap water until the pH of the wash water was ~7, rinsed with DI water three times, and dried in an oven at 60 ℃ overnight.

To carry out the optimization, three factors were varied: (1) concentration of NaOH (%NaOH), (2) temperature of the oil bath, and (3) reaction time. Three levels were selected for each factor. For %NaOH, higher concentrations than those for deproteination[36] were desirable, so 25, 30, and 35 wt% were selected, with the limit of 35 wt% based on existing reports for ChNW preparation.[39] For the temperature, 110, 125, and 140 ℃ were selected, which were higher than previously reported[15,39] to shorten the deacetylation time for consideration of process economic constraints, with the upper limit of 140 ℃ where the 35 wt% NaOH solution began to boil. For the reaction time, 60, 100, and 140 min were selected with a minimum of 60 min to provide enough time for deacetylation[39] and a limit of 140 min to keep the levels evenly spaced. These three-factor three-level experimental conditions were designed using an L9 orthogonal array (ChNW1 to 9), summarized in rows 1-9 in Table 1. ChNWopt1 was treated under the optimal conditions (35 wt% NaOH, 140℃, 140 min) determined by the Taguchi method, and ChNWopt2 was treated under

more aggressive conditions (40 wt% NaOH, 155°C, 140 min) extrapolated beyond the original orthogonal design framework, shown in rows 10 and 11 in Table 1, respectively.

Preparation of film samples

The deacetylated chitin was homogenized into a 0.5 wt% ChNW suspension and then used for spray coating to produce solid coatings. ChNW and CNC suspensions were coated on the CA substrate successively to form a bilayer-coated film (CA-ChNW-CNC) using a setup shown in Figure S1. For comparison, CA films coated with only ChNW or CNC were prepared in the same method, and they are referred to as CA-ChNW and CA-CNC. Full details of homogenization and spray coating are shown in the Supporting Information.

Characterization

For the suspensions, the size of ChNW was characterized using an atomic force microscope (AFM; Dimension XR, Bruker, UK). The crystallinity index of ChNW was characterized by X-ray diffraction (XRD) and calculated using an empirical equation.[40] The DA of each ChNW suspension was characterized by potentiometric titration using a pH meter (Seven Excellence S400, Mettler Toledo, USA).[22] Additional details of AFM, XRD, and potentiometric titration are shown in the Supporting Information. The zeta potential of each 0.025 wt% ChNW suspension (diluted with pH = 3 HOAc solution) was measured using a Zetasizer Nano ZS (Malvern Panalytical, UK). The suspension viscosity was characterized using a rheometer (AR 2000ex, TA Instruments, USA) at room temperature (~23 °C) by using a 25-mm-in-diameter parallel plate fixture with a 500 μm gap. The size and the viscosity of the 0.5 wt% CNC suspension, and the zeta potential of 0.025 wt% CNC suspension which was diluted with 5 mM NaCl solution were characterized as described above.

The thicknesses of coated and uncoated films were measured with a micrometer (Coolant Proof Micrometer Series 293, Mitutoyo, USA) at ten different points for each sample. The oxygen permeability (OP) values were measured by using an OX-TRAN 1/50 instrument (MOCON, USA) at 23 °C, 50% relative humidity (RH) for the O_2 feed side, and 0% RH for the nitrogen permeant side, which the coating was exposed to, under convergence mode. The water vapor transmission rate (WVTR) was measured by using a PERMATRAN-W 1/50 instrument (MOCON, USA) at 23 °C and 50% RH under convergence mode, where the coating was exposed to the dry side at 5% RH. The mechanical properties of the films were measured under biaxial tension applied with an indenter using a custom high-throughput mechanical characterization (HTMECH) instrument.[41] The cross-sectional structure was characterized by scanning electron microscopy (SEM; SU8010, Hitachi High-Tech Corp., Japan). The cross-sectional element distribution was analyzed by Energy dispersive X-ray spectroscopy (EDS). Full details of HTMECH, SEM and EDS are shown in the Supporting Information.

Statistical analysis

To conduct the multivariable optimization for minimizing the OP of the coated film, the Taguchi method was applied to determine the parameter effect of each level of each factor in the chitin deacetylation step. The Taguchi method is widely applied to reduce the number of experiments required for multivariable optimization by using an orthogonal array of factors that are simultaneously varied in each experiment.[42] The logarithmic form of the signal-to-noise ratio (S/N) from each test was used as a quantitative measure of film performance, where a maximal S/N corresponds to minimum OP. The percentage contribution of each factor was also determined. Full details are provided in the Supporting Information.

RESULTS AND DISCUSSION

Properties of the suspensions and dried films

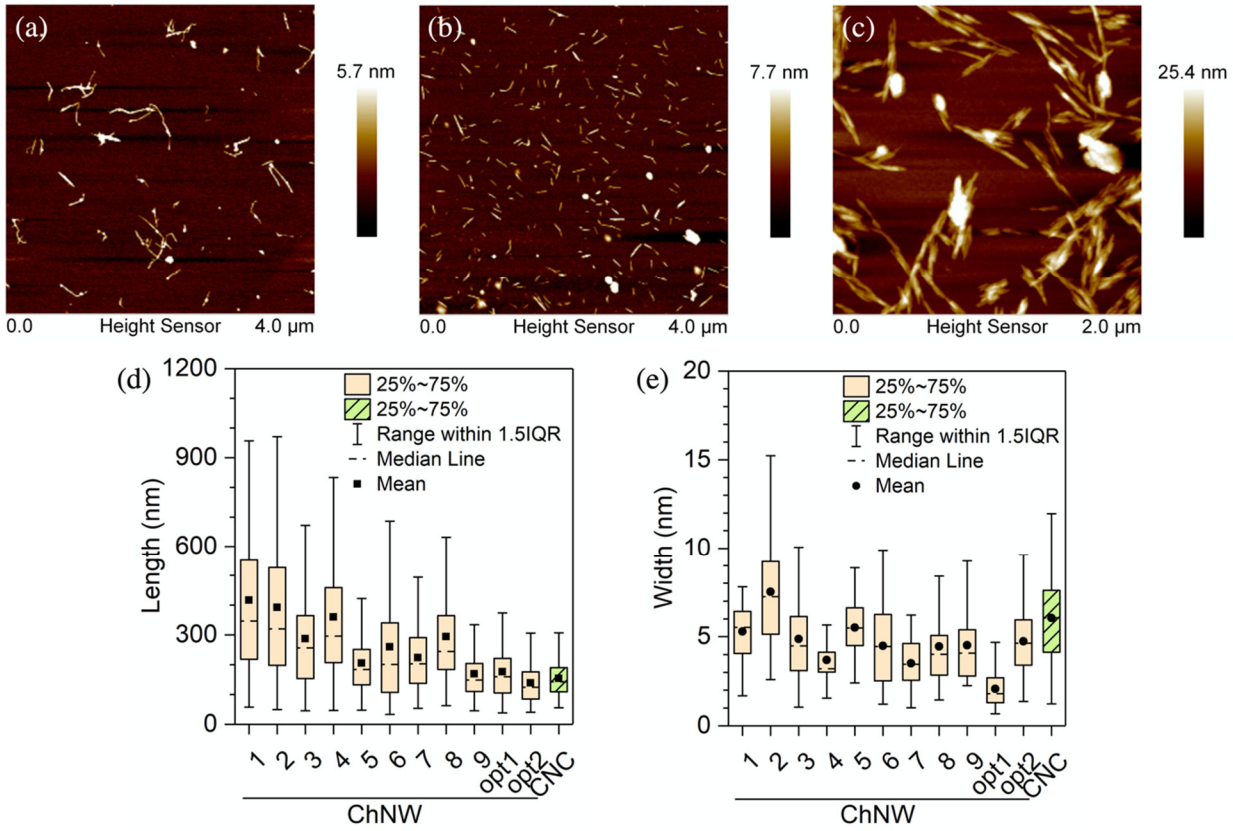

Figure 1. AFM height images of fibers from diluted (a) ChNW1, (b) ChNWopt2, and (c) CNC suspensions. The distributions of (d) the length and (e) the width of the ChNW (non-patterned shading) and CNC (patterned shading) samples, including and the average length (square) or width (circle). The interquartile range (IQR) is the distance between the upper (75%) and lower (25%) quartiles of the dataset.

The size of ChNWs characterized by AFM (Figure 1a-c, Figure S2) was significantly influenced by the deacetylation conditions. The length and the width of ChNWs and CNCs are shown in Figure 1d-e. Size distributions of each ChNW suspension are shown in Figure S3 and Figure S4. The average length of ChNWs decreased from 400±300 nm to 140±70 nm and the range

of lengths was narrowed as the treatment conditions became more aggressive, i.e., higher %NaOH, higher temperature, and longer time. For ChNW treated under less aggressive conditions (i.e., ChNW1, 2, and 4), a small fraction of long fibers (~1.5 μm) remained, shown in Figure S3a. During deacetylation the amide bonds are hydrolyzed, causing both the crystalline region and the amorphous region of the nanofibrils to be deacetylated. Because the hydrolysis takes place faster in the amorphous region than in the crystalline region, the local DA of the amorphous region is lower than that of the crystalline region.[43,44] Thus, similar to chitosan, the highly deacetylated amorphous region is soluble in acidic solution, which is hypothesized to cause the decrease in the length of nanowhiskers observed here. The NaOH-catalyzed hydrolysis of glycosidic bonds within a chitin chain can also significantly shorten its length.[37] The width, on the other hand, was not significantly affected by the treatment conditions and the average values (from 2.1±1.0 nm to 7.5±3.1 nm) were close to the diameter of a typical chitin nanofibril (2-5 nm).[45] The dimensions of the CNC particles used for the top layer, used as received, had an average length of 150±60 nm and an average width of 6.0±2.6 nm, consistent with other reports in the literature.[12]

The values of DA and zeta potential, which reflected the surface charge of the ChNWs, and the calculated surface charge densities are shown in Table 1. The deacetylation conditions within the original orthogonal design had no significant influence on the DA and zeta potential of ChNW1 to 9, which had an average DA of 89.2±3.5% and an average zeta potential of +47.2±1.6 mV. For ChNWopt1 and opt2, the DA decreased to 75.1±1.5% and 76.8±2.8%, respectively, and the zeta potential increased to +54.8±0.6 mV and +58.1±2.3 mV, respectively. Since nanoparticles with zeta potential values greater than +30 mV or lower than –30 mV can be considered to have good stability in suspension,[46] all suspensions in this work were considered stable, including the CNC suspension with a zeta potential of –34.9±0.7 mV (pH = 7, ionic strength of 6 mM). The

surface charge densities were calculated based on the size and the DA, shown in the Supporting Information. For ChNW1 to opt1 within the 3-factor 3-level design, the surface charge density ranged from 7.9±3.4 mC/m^2 to 29.1±14.3 mC/m^2, where the calculated results were proportional to the ChNW width and no significant trend was observed. ChNWopt2 had a higher surface charge density of 38.7±13.9 mC/m^2. The surface charge of ChNWs is expected to increase as the deacetylation conditions become more aggressive. Because the heterogeneous hydrolysis exhibits first-order reaction kinetics,[37] the reaction rate is proportional to the concentration of NaOH. Thus, more acetyl groups were removed with increased NaOH concentration and with an increase in reaction time. Also, because the deacetylation is an endothermic reaction,[47] the final thermodynamically achievable conversion increases with an increasing temperature. These influences were not obvious within the 3-factor 3-level design framework (ChNW1 to opt1) mainly because of the limited range of variation of selected levels.

Table 1. Summary of experimental conditions and resulting properties of ChNW suspensions

ChNW[1]	%NaOH	T (°C)	Time (min)	DA (%)	Zeta potential[2] (mV)	Surface charge density (mC/m^2)	Crystallinity index (%)
1	25	110	60	88.8±1.4	+46.4±0.4	20.6±6.4	84
2	25	125	100	88.8±3.1	+45.7±0.8	29.1±14.5	85
3	25	140	140	93.1±0.8	+46.7±0.8	11.6±6.0	83
4	30	110	100	93.7±1.9	+47.6±0.5	7.9±3.5	85
5	30	125	140	85.7±1.5	+46.3±1.1	27.5±7.5	84
6	30	140	60	93.4±1.0	+46.4±1.1	10.1±5.1	84
7	35	110	140	86.5±1.1	+49.2±1.3	16.4±6.1	83
8	35	125	60	89.0±0.8	+46.0±0.8	16.9±7.6	82
9	35	140	100	84.1±1.7	+50.6±2.0	25.1±12.8	80
opt1	35	140	140	75.1±1.5	+54.8±0.6	18.4±8.7	69
opt2	40	155	140	76.8±2.8	+58.1±2.3	38.7±14.1	29

[1] ChNW1 to 9 were the original orthogonal design. The 'opt1' sample was prepared under optimal conditions as determined using the Taguchi method, and 'opt2' was prepared under more aggressive conditions extrapolated outside the range of the original orthogonal design.

[2] The zeta potential for 0.025 wt% ChNW was measured at pH = 3 and ionic strength of 2 mM.

The XRD patterns for ChNWs are shown in Figure S5 and the crystallinity indices (CrIs) for the ChNWs are summarized in Table 1. The peaks at 2θ = 9°, 19°, and 23° correspond to the (020), (110), and (130) crystallographic planes, respectively.[48] In previous reports using powdered chitin samples,[28,49] there are additional peaks indexed as (021), (120), and (013) at 2θ = 13°, 21°, and 26.4°, beyond the peaks observed in this work. Such peaks were not observed here probably because the chitin in this work was chemically treated for deacetylation and was separated into discrete nanowhiskers by high-pressure homogenization before characterization. Considering that the CrIs have a random uncertainty of 2-4% (not shown in the table), no significant variance was observed in the CrIs of ChNW1 to 9, which had an average of 83±2%. This indicated that the change in deacetylation conditions within the original orthogonal design did not significantly influence the crystalline structure of the ChNWs. In comparing ChNW9, opt1, and opt2, the CrI decreased from 80% to 69 % and 29%, respectively, as the deacetylation conditions became more aggressive outside of the original orthogonal design. The peaks of planes (020) and (110) almost disappeared for ChNWopt2 (Figure S5), which indicated that the ChNWopt2 had a less ordered structure due to a significant decrease in crystallinity.

The viscosities of ChNW and CNC suspensions at different shear rates are shown in Figure S6. ChNW1 to 9 and opt1 showed shear thinning behavior, while ChNWopt2 and CNC behaved as Newtonian fluids at a shear rate greater than 25 s^{-1} and 60 s^{-1}, respectively. The ChNWopt2 and the CNC had shorter lengths than the other samples, which resulted in fewer entanglements. This is indicated by the AFM images in Figure S2, where ChNW1 to 8 had longer length with visible entanglements in the dried state, and ChNWopt2 and CNC did not have these features. As a result, the microstructure of the unentangled suspensions remains relatively unchanged by shear flow. An

overall trend is that the viscosity of ChNW suspensions increased with an increasing aspect ratio of the nanowhiskers. This trend agrees with a previous report for CNC and CNF suspensions.[50]

Table 2. Thicknesses and mechanical properties of coated or uncoated CA films

Film		Thickness (μm)	Ultimate tensile strength (MPa)	Failure strain (%)
CA		77±1	36.0±0.9	22.7±2.7
CA-ChNW*x*-CNC, where *x* =	1	80±1	33.3±1.2	21.6±1.1
	2	81±1	31.9±0.9	19.0±2.7
	3	83±2	32.3±1.4	20.5±1.4
	4	79±1	33.6±1.1	23.6±1.8
	5	83±2	31.1±0.9	22.7±1.4
	6	81±1	30.6±1.8	22.1±3.4
	7	82±1	30.9±1.7	23.4±3.8
	8	83±1	31.9±1.0	21.6±1.0
	9	79±2	33.5±1.0	23.5±2.6
	opt1	82±1	33.3±1.2	22.1±1.5
	opt2	80±1	32.5±0.9	20.9±1.5

The mechanical properties of the coated or uncoated films are shown in Table 2. The ultimate tensile strength (UTS) and the failure strain (FS) of the coated films were not significantly influenced by the deacetylation conditions for ChNWs. A possible explanation is that the coating comprised only ~5% of the total thickness, and the UTS and FS of the substrate are higher than those of neat CNC and ChNW films,[51] thus the substrate contributed more to the mechanical properties of coated films. The average UTS of the coated films was 32.3±1.1 MPa, which was ~10% lower than that of the neat CA film (36.0±0.9 MPa). As discussed in a previous report of a similar multilayer film,[22] the decrease of UTS might be the result of relative brittleness of the CNC and ChNW layers and residual stress between the coating and the substrate. The factors are known to lead to reduced UTS of multilayered films.[52] However, in terms of the FS, most of the coated films were not significantly different from the neat CA film, and the average FS for all films was

22.0±1.4%. Representative stress-strain curves of the coated and uncoated films are shown in Figure S7. Additional analyses on the statistical significance for UTS and FS are available in Table S2 and Table S3.

To evaluate the effects of deacetylation on the barrier performance of CA-ChNW-CNC films, ChNW and CNC were spray-coated sequentially on CA: ChNW was first applied to CA followed by CNC application to the ChNW layer. The optical image for the uncoated CA and a typical CA-ChNW-CNC film is shown in Figure 2a. The thicknesses of the films are shown in Table 2, and average values for the coated and uncoated films were 81±2 μm and 77±1 μm, respectively. Considering that the same volumes of ChNW and CNC suspensions with identical solid content were sprayed, the bilayer coating contained ~2 μm each of ChNW and CNC. Cross-sectional SEM images for the coated film (Figure 2b-c and Figure S8) showed layered lamellar structure in the ChNW-CNC coating, but the ChNW-CNC interface was unobservable. The multilayer structure was verified by EDS line scan results (Figure S9), where the peak of the N-signal indicated the center of the ChNW layer, and the peaks of the S- and Na-signals indicated the center of the CNC layer. For CA-ChNWopt2-CNC film (Figure S9f), however, the peaks for the S- and Na-signals were unexpectedly closer to the CA surface than that of the N-signal. This suggests mixing of CNC with ChNWopt2 at their interface. One possible reason is that the ChNWopt2 had shorter average length than the other ChNW samples, allowing them to diffuse and penetrate the CNC layer more easily when the ChNW layer was rewetted by the CNC suspension. Another possibility is that ChNWopt2 had the highest surface charge density among all ChNW samples. This suggests stronger electrostatic attraction between CNC and ChNWopt2 compared to other ChNWs, which probably promotes interdiffusion of ChNWopt2 and CNC.

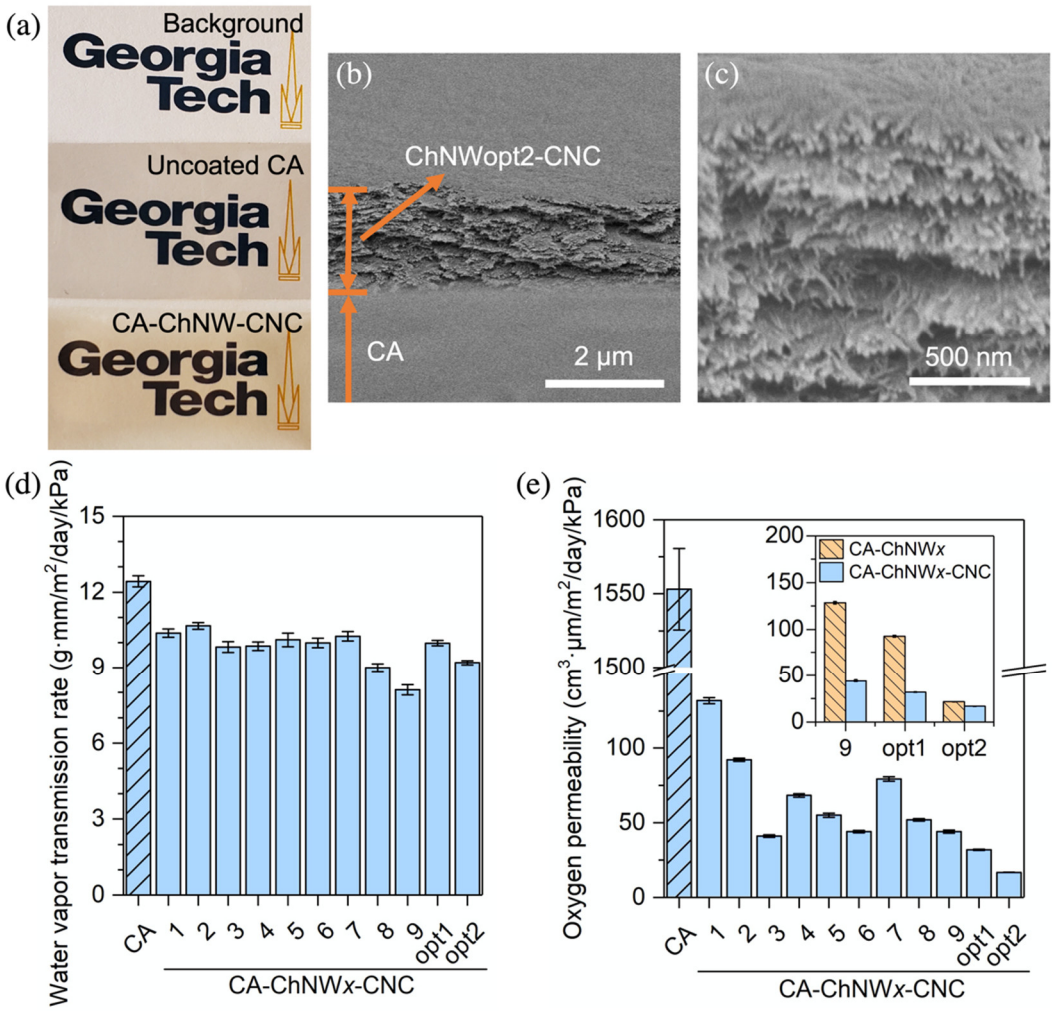

Figure 2. Structure and gas barrier properties for coated and uncoated CA films. (a) Optical images for the uncoated CA and a typical CA-ChNW-CNC film. SEM images for the cross-sections of (b) the CA-ChNWopt2-CNC film with an exposed top surface and (c) the ChNWopt2-CNC coating at a higher resolution. (d) Normalized water vapor transmission rate and (e) oxygen permeability (OP) of the neat CA film (patterned) or CA-ChNW*x*-CNC films (non-patterned), and the inset of e is the comparison of OP between selected single-layer-coated films and corresponding CA-ChNW*x*-CNC films, where *x* indicates the serial number of ChNW.

The normalized WVTR of the coated and uncoated films are shown in Figure 2d. The WVTR of the CA-ChNW-CNC films decreased by around 20% compared to neat CA film, and the variation in the WVTR values of the coated films is small (~10%). In a previous report of TEMPO-oxidized-CNF-coated PLA or PET films,[53] similar results were found where the WVTR was not significantly influenced by the fiber length. This is possibly because the WVTR is mainly dependent on the moisture content of the film,[19] and the coated films in this work which were dried and stored under the same conditions had similar moisture content. As a result, the focus of the remainder of this paper is on the control of OP.

The values of OP of the CA-ChNW-CNC bilayer films generally decreased as the deacetylation conditions became more aggressive, as shown in Figure 2e. For example, for ChNW1 to 3, the %NaOH was kept constant, but the treatment temperature and time were systematically increased, and the OP of the coated film decreased. The OP values of selected single-layer-coated films (CA-ChNW and CA-CNC) are shown in the inset of Figure 2e, and their thicknesses are shown in Table S4. The OP of CA-ChNW samples decreased from 128 $cm^3 \cdot \mu m/m^2/day/kPa$ (ChNW9) to 21.5 $cm^3 \cdot \mu m/m^2/day/kPa$ (ChNWopt2) as the deacetylation conditions became more aggressive. Also, CA-ChNW-CNC bilayer films had a lower OP than its corresponding single layer CA-ChNW or CA-CNC (102 $cm^3 \cdot \mu m/m^2/day/kPa$) film. This is attributed to the densification at the ChNW-CNC interface caused by electrostatic attraction and the interdiffusion when the ChNW layer was rewetted by the CNC suspension. These results verified the superior O_2 barrier performance resulting from combining ChNW and CNC as multilayers compared to single coating layers, as well as the distinct improvements from more aggressive deacetylation of the ChNW.

Focusing initially on the original orthogonal design of ChNW1 to 9, the OP of the CA-ChNW-CNC films ranged from 132±2 $cm^3 \cdot \mu m/m^2/day/kPa$ (ChNW1) to 41.0±0.9 $cm^3 \cdot \mu m/m^2/day/kPa$ (ChNW3), which was a 91-97% decrease in comparison to the neat CA film whose OP was 1553±27 $cm^3 \cdot \mu m/m^2/day/kPa$. It is interesting that ChNW1 to 9 samples with similar surface charge (i.e., DA and zeta potential) and similar CrI values still resulted in significant variation in OP of the CA-ChNW-CNC films. This suggests that the size of ChNWs played a dominant role in influencing the OP of the coated film. In particular, the overall trend showed that CA films coated with bilayers containing shorter ChNWs had lower OP. For example, for ChNW1, 2, and 8 with similar values of DA, and for ChNW1, 2, and 4 with similar CrI, shorter ChNW led to a lower OP. A possible reason is that it is easier for shorter, unentangled whiskers to orient with CNCs to optimize electrostatic attraction, leading to denser packing in the coating. This conclusion contradicts a previous study of TEMPO-oxidized-CNF-coated PET films, in which longer CNFs led to a better O_2 barrier property.[53] However, the aforementioned study explored the coating of single CNF layers rather than multilayers of oppositely charged materials. Also, the average lengths for TEMPO-oxidized-CNFs were 200 nm, 680 nm, and 1100 nm, which was beyond the range of length of nanowhiskers in this work (from 140 nm to 400 nm).

Statistical analysis

In this work, our primary aim was to optimize the chitin deacetylation step to produce bilayer coatings of ChNW-CNC on CA that result in the lowest OP values. Only the results from the original orthogonal framework (ChNW1 to 9) were used for statistical analysis to predict the optimal processing conditions. Independent samples were prepared based on that prediction (ChNWopt1 and opt2) for comparison.

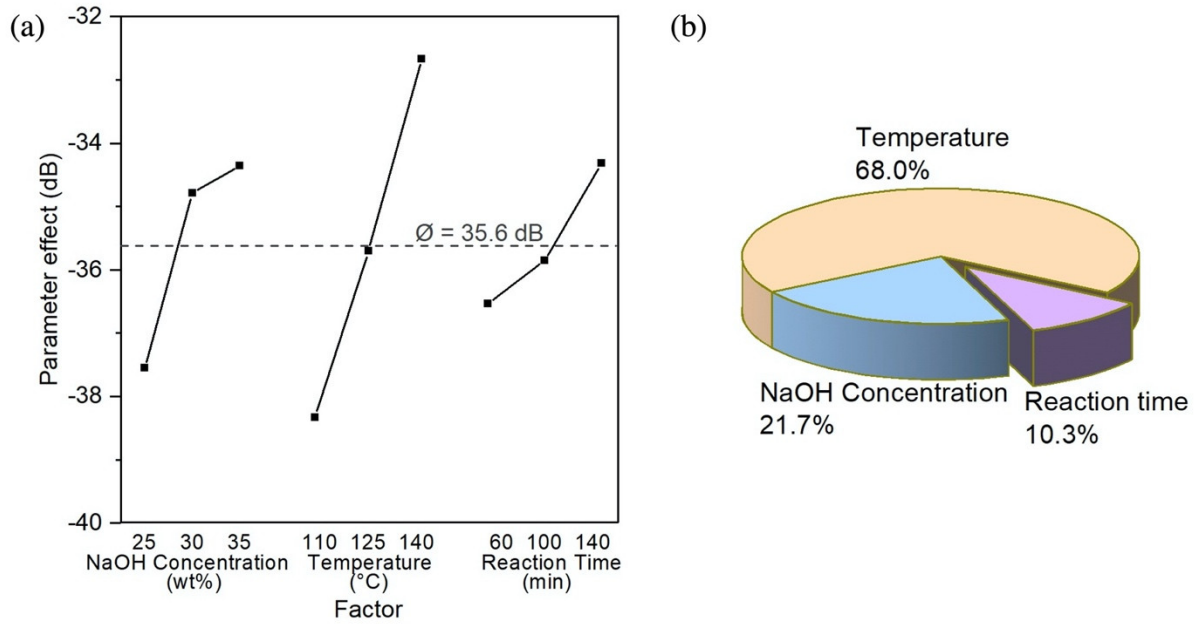

Figure 3. Results of Taguchi analysis: (a) parameter effects, where the greatest value indicates the optimal level and ∅ is the average of all the nine values of parameter effects, and (b) percentage effect contribution of each parameter.

When applying the Taguchi method, the optimal levels of the three factors (%NaOH, temperature, reaction time) for minimizing the OP (i.e., maximizing signal to noise, S/N) were found using the parameter effect (*K*), as shown in Figure 3a. It is observed that the $K_{\%NaOH}$ increased with the %NaOH. The $K_{Temperature}$ increased with a relatively constant slope from 110 ℃ to 140 ℃, and its range was larger than the *K*'s of the other two factors. The K_{Time} increased with an increasing slope, and its range was smaller than those of %NaOH and temperature. For each factor, the level with the largest *K* was determined as the optimal level because *K* is an averaged logarithmic form of S/N as calculated using the equations in the Supporting Information, and a larger S/N is equivalent to a smaller OP.[54] Thus, the optimal conditions for the deacetylation step

in the 3-factor 3-level design were 35 wt% NaOH, 140℃, and 140 min, corresponding to sample ChNWopt1.

The percentage effect of the contribution of each factor (ρ) (Figure 3b) was used for finding the degree of influence of the factors on the OP. The temperature has the most significant influence (68.0%) on the OP of the resulting film, followed by %NaOH (21.7%) and reaction time (10.3%). This conclusion was verified by comparing ChNW1 to 3, 4 to 6, and 7 to 9 separately, where the OP decreased with an increasing treatment temperature, even though the reaction time was not controlled. Combining the conclusion that the ChNWs with a shorter length let to coatings with lower OP, an increase in reaction temperature played a dominant role in shortening the length of ChNWs. As a general guideline, the factors with ρ smaller than 5% are considered to have negligible impacts on the target parameter, because their contributions are lost in uncertainty.[38] In this work, each parameter contributed greater than 5%, so each of the three factors was significant. The OP for a CA-ChNW-CNC film with ChNW prepared under the optimal conditions (ChNWopt1) can be predicted using equation 6 to 9 in the Supporting Information, which was 32.4 $cm^3 \cdot \mu m/m^2/day/kPa$.

Optimization of oxygen permeability

To verify the determined optimal conditions, one batch of ChNW was prepared under the opt1 conditions. The OP for CA-ChNWopt1-CNC was 31.8±0.3 $cm^3 \cdot \mu m/m^2/day/kPa$, which was only 2% lower than the predicted value of 32.4 $cm^3 \cdot \mu m/m^2/day/kPa$. This result confirms the estimation based on the optimal deacetylation conditions.

Note that the optimal levels represented the most aggressive conditions in the 3-factor 3-level framework, suggesting that further increases in temperature and %NaOH could lead to a further reduction in OP. To address this hypothesis, one batch of ChNW was prepared with a more

concentrated NaOH solution (40 wt%) at a higher temperature (155 °C). The reaction time was kept at 140 min because its relatively minor effect on the OP from the statistical analysis. The resulting ChNW is referred to as opt2. The OP for CA-ChNWopt2-CNC was 16.7±0.1 $cm^3 \cdot \mu m/m^2/day/kPa$. In comparison to the neat CA film, the OP decreased up to 99% after the addition of the ChNW-CNC coated bilayer, indicating the excellent O_2 barrier property of the ChNW-CNC coating. The coated films meet the OP requirement for food products packaging, which can range from 16 to 3200 $cm^3 \cdot \mu m/m^2/day/kPa$, i.e., 20-4000 $cm^3/m^2/day$ of O_2 transport rate, for bakery products packaging.[19] Increases in thickness can lead to additional decreases in O_2 transport rate. Notably, the optimal OP value of 16.7 $cm^3 \cdot \mu m/m^2/day/kPa$ for CA-ChNWopt2-CNC is significantly lower than that of polyethylene (i.e., 490-2000 $cm^3 \cdot \mu m/m^2/day/kPa$) and is comparable to commercially available biaxially oriented PET (i.e., 9-24 $cm^3 \cdot \mu m/m^2/day/kPa$).[55] However, there is still room for improvement in oxygen barrier property compared to that of PVDC (i.e., 0.1-3 $cm^3 \cdot \mu m/m^2/day/kPa$).[55]

The CA-ChNWopt2-CNC film had a lower OP than all other CA-ChNW-CNC films. This is hypothesized to be the result of a denser interface between ChNWopt2 and CNC, attributed to the shorter length and higher surface charge of ChNWopt2, facilitating interpenetration of ChNWopt2 with the CNC layer and forming stronger electrostatic attraction at their interface. This hypothesis is supported by the EDS result shown in Figure S9. It is also interesting to find that the ChNW with lower crystallinity had better O_2 barrier property by comparing ChNW9, opt1, and opt2. Previous reports in the literature demonstrate that polymers with a higher degree of crystallinity usually have a lower OP.[56] One possibility is that crystallinity plays a dominant role in semi-crystalline molecular polymers where gas molecules diffuse primarily through amorphous regions.[57] However, in a coating of particulate fibers whose size is much larger than a molecular

polymer, the process of O_2 transport is dominated by transport through voids between particles. Thus, achieving more densely packed nanofibers is the critical step to lower gas permeability.[28] Therefore, minimizing the size of the chitin nanowhiskers is likely a dominant factor in limiting O_2 permeation. Decreasing the DA of ChNW, increasing the fiber charge density, will also improve the electrostatic attraction between ChNWs and CNCs and lower the interfiber free volume.

The optimal CA-ChNWopt2-CNC film had a lower OP values than previous studies which utilized similar materials. Satam et al.[22] deposited ChNF and CNC layers on PLA substrate by spray coating, and the resulting film had an OP of ~20 $cm^3 \cdot \mu m/m^2/day/kPa$ at 50% RH. The deacetylation conditions in Satam et al.'s work (5% NaOH, refluxing for 48 h) were not optimized and the ChNFs were significantly longer than ChNWs in this work. Nevertheless, the CA-ChNW-CNC films in this work had higher OP values than those in other previous studies. For example, Kim et al.[21] prepared coated PET film (50 μm) by alternatively spraying ChNW and CNF, and a sample with 20 bilayers of ChNW-CNF (2.62 μm in total) had an OP of 0.25 $cm^3 \cdot \mu m/m^2/day/kPa$. However, the tests in that work were carried out under dry conditions (0% RH), while the work presented here used 50% RH. The OP of cellulose and chitin materials are known to increase with humidity,[19,22] making the comparison at different humidity values difficult. The work of Kim et al. suggests that spray-coated samples prepared with more bilayers, each of which is thinner, had more ChNW-CNF interfaces, which may lead to a denser structure of the coatings. An additional comparison can be made to Li et al.[58] who fabricated CNC (1.5 μm)-coated PET film (12 μm) by rod coating with an OP of ~0.27 $cm^3 \cdot \mu m/m^2/day/kPa$ (0% RH). Because that film was dried at room temperature, its drying rate was slower than that of the heated drying process (65°C) in this work. A chiral nematic structure in the CNC coating can be obtained by slow evaporation,[59] which

leads to alignment and densification of CNCs and decreased the OP of the film.[17] The PET substrate in that work had a significantly lower OP than the CA substrate in this work, and PET's contribution to the overall mass transfer resistance could be significant.[19,22]

The improved performance in ChNW-CNC coatings is achieved by intensification of the deacetylation process, which will result in increased process energy and material consumption. While a technoeconomic analysis of ChNW production is not available, we use a recent analysis for chitosan production, which breaks out the energy use for the deacetylation step, as a proxy for ChNW.[60] We estimate that the increased deacetylation intensity (time, T and % NaOH) that results in the smallest OP in this work would lead to a 250% increase in the deacetylation process energy in comparison to the least aggressive deacetylation conditions in this work. However, the magnitude of this deacetylation energy, required to produce a 25 μm ChNWopt2 film, would be only ~0.17 MJ/m^2. While the total energy embodied in producing ChNW-CNC coated films is unavailable, we can gain insight into the significance of the increased deacetylation energy by comparing it to PET. From published analyses of PET we estimate the energy embodied is 2.8 MJ/m^2 for an equivalent thickness PET film.[61] Details of the calculation are shown in the Supporting Information. This simplified analysis does not consider CNC or the ChNW homogenization step, but it illustrates the magnitude of the trade-off in deacetylation process energy. These values motivate future complete technoeconomic and lifecycle comparisons of conventional versus renewable barrier packaging.

CONCLUSIONS

In summary, we have shown for the first time that by tuning the chitin deacetylation conditions, the O_2 barrier property of CA films coated with bilayers of ChNW-CNC is successfully enhanced, bringing them to values near that of commercially available biaxially oriented PET.

Using the Taguchi method, the effects of chitin deacetylation conditions (%NaOH, temperature, and reaction time) on the OP of coated films was studied. The optimal conditions of the deacetylation step were determined to be 35 wt% NaOH, 140 °C for the oil bath, and 140 min. The temperature was the dominant factor (68.0%) that influenced the OP of the CA-ChNW-CNC films, followed by %NaOH (21.7%) and the reaction time (10.3%). More aggressive deacetylation significantly shortened the length of ChNWs, and we hypothesize this facilitates the formation of denser coatings with lower OP values when ChNWs and CNCs interact electrostatically during drying. ChNW prepared under optimal conditions (ChNWopt1) resulted in bilayer-coated films with better O_2 barrier properties (31.8 $cm^3 \cdot \mu m/m^2/day/kPa$) than ChNW1 to 9, in agreement with the predicted value. By extrapolating beyond the 3-factor 3-level design space and making the deacetylation conditions more aggressive (40 wt% NaOH, 155℃, 140 min), the OP of the coated film was further lowered to 16.7 $cm^3 \cdot \mu m/m^2/day/kPa$, which is comparable to that of commercial oriented PET film.

This work improved the sustainability of producing an oxygen barrier packaging material by utilizing materials sourced from plants and food waste. Renewably sourced CA-ChNW-CNC film is a potential substitute for common petroleum-based O_2 barriers. Nevertheless, although the coated film had lower WVTR than the uncoated CA film, there is still much room for improvement for the application in food packaging. This might be addressed by adding fillers, such as nanoclay[62] and metal oxide nanoparticles,[63,64] into either suspension or controlling the moisture content,[65] or layering with a moisture barrier material, and such solutions would also be helpful to enhance the O_2 barrier property at the same time.[16,66]

ACKNOWLEDGMENT

The authors acknowledge the Department of Energy (DOE) for financial support of this work (EE0008494). This work was authored in part by the National Renewable Energy Laboratory (NREL), operated by Alliance for Sustainable Energy, LLC, for the U.S. DOE under Contract No. DE-AC36-08GO28308. This work was performed in part at the Georgia Tech Institute for Electronics and Nanotechnology, a member of the National Nanotechnology Coordinated Infrastructure (NNCI), which is supported by the National Science Foundation (ECCS-2025462).

ASSOCIATED CONTENT

Supporting Information

Additional experimental details, statistical analysis, supplementary results (i.e., AFM images, size distributions, XRD patterns, viscosity, stress-strain curves, SEM images, EDS results, statistical significance analyses for mechanical properties), and details of calculating the surface charge density and the energy consumption.

REFERENCE

1. Kausar, A., A review of high performance polymer nanocomposites for packaging applications in electronics and food industries. *J Plast Film Sheet* **2020,** *36* (1), 94-112. DOI: 10.1177/8756087919849459

2. Zhang, L. M.; Yu, D. W.; Regenstein, J. M.; Xia, W. S.; Dong, J. L., A comprehensive review on natural bioactive films with controlled release characteristics and their applications in foods and pharmaceuticals. *Trends Food Sci. Technol.* **2021,** *112*, 690-707. DOI: 10.1016/j.tifs.2021.03.053

3. Majid, I.; Thakur, M.; Nanda, V., Innovative and Safe Packaging Technologies for Food and Beverages: Updated Review. In *Innovations in Technologies for Fermented Food and*

Beverage Industries, Panda, S. K.; Shetty, P. H., Eds. Springer International Publishing: Cham, 2018; pp 257-287. DOI: 10.1007/978-3-319-74820-7_13

4. Barlow, C. Y.; Morgan, D. C., Polymer film packaging for food: An environmental assessment. *Resour. Conserv. Recycl.* **2013,** *78*, 74-80. DOI: 10.1016/j.resconrec.2013.07.003

5. Rhim, J. W.; Park, H. M.; Ha, C. S., Bio-nanocomposites for food packaging applications. *Prog. Polym. Sci.* **2013,** *38* (10-11), 1629-1652. DOI: 10.1016/j.progpolymsci.2013.05.008

6. Hopewell, J.; Dvorak, R.; Kosior, E., Plastics recycling: challenges and opportunities. *Philos. Trans. R. Soc. B* **2009,** *364* (1526), 2115-2126. DOI: 10.1098/rstb.2008.0311

7. Otoni, C. G.; Avena-Bustillos, R. J.; Azeredo, H. M. C.; Lorevice, M. V.; Moura, M. R.; Mattoso, L. H. C.; McHugh, T. H., Recent Advances on Edible Films Based on Fruits and Vegetables-A Review. *Comprehensive Reviews in Food Science and Food Safety* **2017,** *16* (5), 1151-1169. DOI: 10.1111/1541-4337.12281

8. Barnes, D. K. A.; Galgani, F.; Thompson, R. C.; Barlaz, M., Accumulation and fragmentation of plastic debris in global environments. *Philos. Trans. R. Soc. B* **2009,** *364* (1526), 1985-1998. DOI: 10.1098/rstb.2008.0205

9. Tullo, A. H. The cost of plastic packaging 2016, p. 33-37. https://cen.acs.org/articles/94/i41/cost-plastic-packaging.html (accessed 2021-07-06).

10. Lavoine, N.; Desloges, I.; Dufresne, A.; Bras, J., Microfibrillated cellulose - Its barrier properties and applications in cellulosic materials: A review. *Carbohydr. Polym.* **2012,** *90* (2), 735-764. DOI: 10.1016/j.carbpol.2012.05.026

11. Ifuku, S.; Saimoto, H., Chitin nanofibers: preparations, modifications, and applications. *Nanoscale* **2012,** *4* (11), 3308-3318. DOI: 10.1039/c2nr30383c

12. Moon, R. J.; Martini, A.; Nairn, J.; Simonsen, J.; Youngblood, J., Cellulose nanomaterials review: Structure, properties and nanocomposites. *Chem. Soc. Rev.* **2011,** *40*, 3941-3994. DOI: 10.1039/c0cs00108b

13. Zeng, J. B.; He, Y. S.; Li, S. L.; Wang, Y. Z., Chitin Whiskers: An Overview. *Biomacromolecules* **2012,** *13* (1), 1-11. DOI: 10.1021/bm201564a

14. Wu, J.; Zhang, K.; Girouard, N.; Meredith, J. C., Facile Route to Produce Chitin Nanofibers as Precursors for Flexible and Transparent Gas Barrier Materials. *Biomacromolecules* **2014,** *15* (12), 4614-4620. DOI: 10.1021/bm501416q

15. Fan, Y. M.; Fukuzumi, H.; Saito, T.; Isogai, A., Comparative characterization of aqueous dispersions and cast films of different chitin nanowhiskers/nanofibers. *Int. J. Biol. Macromol.* **2012,** *50* (1), 69-76. DOI: 10.1016/j.ijbiomac.2011.09.026

16. Xia, J. Y.; Zhang, Z.; Liu, W.; Li, V. C. F.; Cao, Y. F.; Zhang, W.; Deng, Y. L., Highly transparent 100% cellulose nanofibril films with extremely high oxygen barriers in high relative humidity. *Cellulose* **2018,** *25* (7), 4057-4066. DOI: 10.1007/s10570-018-1843-y

17. Chowdhury, R. A.; Nuruddin, M.; Clarkson, C.; Montes, F.; Howarter, J.; Youngblood, J. P., Cellulose Nanocrystal (CNC) Coatings with Controlled Anisotropy as High-Performance Gas Barrier Films. *ACS Appl. Mater. Interfaces* **2019,** *11* (1), 1376-1383. DOI: 10.1021/acsami.8b16897

18. Liu, Y. Z.; Matuana, L. M., Surface texture and barrier performance of poly(lactic acid)-cellulose nanocrystal extruded-cast films. *J. Appl. Polym. Sci.* **2019,** *136* (22). DOI: 10.1002/app.47594

19. Wang, J.; Gardner, D. J.; Stark, N. M.; Bousfield, D. W.; Tajvidi, M.; Cai, Z., Moisture and Oxygen Barrier Properties of Cellulose Nanomaterial-Based Films. *ACS Sustain. Chem. Eng.* **2018,** *6* (1), 49-70. DOI: 10.1021/acssuschemeng.7b03523

20. Thuy, V. T. T.; Hao, L. T.; Jeon, H.; Koo, J. M.; Park, J.; Lee, E. S.; Hwang, S. Y.; Choi, S.; Park, J.; Oh, D. X., Sustainable, self-cleaning, transparent, and moisture/oxygen-barrier coating films for food packaging. *Green Chem.* **2021,** *23* (7), 2658-2667. DOI: 10.1039/D0GC03647A

21. Kim, T.; Tran, T. H.; Hwang, S. Y.; Park, J.; Oh, D. X.; Kim, B. S., Crab-on-a-Tree: All Biorenewable, Optical and Radio Frequency Transparent Barrier Nanocoating for Food Packaging. *ACS Nano* **2019,** *13* (4), 3796-3805. DOI: 10.1021/acsnano.8b08522

22. Satam, C. C.; Irvin, C. W.; Lang, A. W.; Jallorina, J. C. R.; Shofner, M. L.; Reynolds, J. R.; Meredith, J. C., Spray-Coated Multilayer Cellulose Nanocrystal-Chitin Nanofiber Films for Barrier Applications. *ACS Sustain. Chem. Eng.* **2018,** *6* (8), 10637-10644. DOI: 10.1021/acssuschemeng.8b01536

23. Yu, Z. Y.; Ji, Y.; Bourg, V.; Bilgen, M.; Meredith, J. C., Chitin- and cellulose-based sustainable barrier materials: a review. *Emergent Mater* **2020,** *3* (6), 919-936. DOI: 10.1007/s42247-020-00147-5

24. Yan, N.; Chen, X., Don't waste seafood waste. *Nature* **2015,** *524* (7564), 155-157. DOI: 10.1038/524155a

25. Barikani, M.; Oliaei, E.; Seddiqi, H.; Honarkar, H., Preparation and application of chitin and its derivatives: a review. *Iran. Polym. J.* **2014,** *23* (4), 307-326. DOI: 10.1007/s13726-014-0225-z

26. Dutta, P. K.; Dutta, J.; Tripathi, V. S., Chitin and chitosan: Chemistry, properties and applications. *J. Sci. Ind. Res.* **2004,** *63* (1), 20-31.

27. Sato, K.; Yamamoto, K.; Kadokawa, J., Preparation of Cationic/Anionic Chitin Nanofiber Composite Materials. *J. Polym. Environ.* **2018,** *26* (9), 3540-3549. DOI: 10.1007/s10924-018-1242-3

28. Duan, B.; Chang, C. Y.; Ding, B. B.; Cai, J.; Xu, M.; Feng, S. C.; Ren, J. Z.; Shi, X. W.; Du, Y. M.; Zhang, L. N., High strength films with gas-barrier fabricated from chitin solution dissolved at low temperature. *J. Mater. Chem. A* **2013,** *1* (5), 1867-1874. DOI: 10.1039/C2TA00068G

29. Swain, S. K.; Dash, S.; Kisku, S. K.; Singh, R. K., Thermal and Oxygen Barrier Properties of Chitosan Bionanocomposites by Reinforcement of Calcium Carbonate Nanopowder. *Journal of Materials Science & Technology* **2014,** *30* (8), 791-795. DOI: 10.1016/j.jmst.2013.12.017

30. Li, F.; Biagioni, P.; Finazzi, M.; Tavazzi, S.; Piergiovanni, L., Tunable green oxygen barrier through layer-by-layer self-assembly of chitosan and cellulose nanocrystals. *Carbohydr. Polym.* **2013,** *92* (2), 2128-2134. DOI: 10.1016/j.carbpol.2012.11.091

31. Wu, Q.; Mushi, N. E.; Berglund, L. A., High-Strength Nanostructured Films Based on Well-Preserved alpha-Chitin Nanofibrils Disintegrated from Insect Cuticles. *Biomacromolecules* **2020,** *21* (2), 604-612. DOI: 10.1021/acs.biomac.9b01342

32. Percot, A.; Viton, C.; Domard, A., Optimization of chitin extraction from shrimp shells. *Biomacromolecules* **2003,** *4* (1), 12-18. DOI: 10.1021/bm025602k

33. Paduretu, C. C.; Isopescu, R. D.; Gijiu, C. L.; Rau, I.; Apetroaei, M. R.; Schroder, V., Optimization of chitin extraction procedure from shrimp waste using Taguchi method and

chitosan characterization. *Molecular Crystals and Liquid Crystals* **2019,** *695* (1), 19-28. DOI: 10.1080/15421406.2020.1723902

34. Peniche, C.; Arguelles-Monal, W.; Goycoolea, F. M., Chitin and Chitosan: Major Sources, Properties and Applications. *Monomers, Polymers and Composites from Renewable Resources* **2008**, 517-542. DOI: 10.1016/B978-0-08-045316-3.00025-9

35. Ahing, F. A.; Wid, N., Optimization of shrimp shell waste deacetylation for chitosan production. *International Journal of Advanced and Applied Sciences* **2016,** *3* (10), 31-36. DOI: 10.21833/ijaas.2016.10.006

36. Younes, I.; Rinaudo, M., Chitin and chitosan preparation from marine sources. Structure, properties and applications. *Mar. Drugs* **2015,** *13* (3), 1133-74. DOI: 10.3390/md13031133

37. Tsaih, M. L.; Chen, R. H., The effect of reaction time and temperature during heterogenous alkali deacetylation on degree of deacetylation and molecular weight of resulting chitosan. *J. Appl. Polym. Sci.* **2003,** *88* (13), 2917-2923. DOI: 10.1002/app.11986

38. Ruefer, H., *Living Without Mathematical Statistics Accurate Analysis, Diagnosis, and Prognosis Based on the Taguchi Method*. 1st ed. 2019.. ed.; Springer: 2019. DOI: 10.1007/978-3-319-99632-5

39. Fan, Y. M.; Saito, T.; Isogai, A., Individual chitin nano-whiskers prepared from partially deacetylated alpha-chitin by fibril surface cationization. *Carbohydr. Polym.* **2010,** *79* (4), 1046-1051. DOI: 10.1016/j.carbpol.2009.10.044

40. Zhang, Y. Q.; Xue, C. H.; Xue, Y.; Gao, R. C.; Zhang, X. L., Determination of the degree of deacetylation of chitin and chitosan by X-ray powder diffraction. *Carbohydr. Res.* **2005,** *340* (11), 1914-1917. DOI: 10.1016/j.carres.2005.05.005

41. Sormana, J. L.; Chattopadhyay, S.; Meredith, J. C., High-throughput mechanical characterization of free-standing polymer films. *Rev. Sci. Instrum.* **2005,** *76* (6), 9. DOI: 10.1063/1.1926967

42. Tsui, K. L., An Overview of Taguchi Method and Newly Developed Statistical-Methods for Robust Design. *Iie Transactions* **1992,** *24* (5), 44-57. DOI: 10.1080/07408179208964244

43. Wang, C.; Esker, A. R., Nanocrystalline chitin thin films. *Carbohydr. Polym.* **2014,** *102*, 151-158. DOI: 10.1016/j.carbpol.2013.10.103

44. Sharples, A., The Hydrolysis of Cellulose and Its Relation to Structure. *Trans. Faraday Society* **1957,** *53* (7), 1003-1013. DOI: 10.1039/tf9575301003

45. Raabe, D.; Sachs, C.; Romano, P., The crustacean exoskeleton as an example of a structurally and mechanically graded biological nanocomposite material. *Acta Mater.* **2005,** *53* (15), 4281-4292. DOI: 10.1016/j.actamat.2005.05.027

46. Bhattacharjee, S., DLS and zeta potential - What they are and what they are not? *Journal of Controlled Release* **2016,** *235*, 337-351. DOI: 10.1016/j.jconrel.2016.06.017

47. He, X.; Li, K.; Xing, R.; Liu, S.; Hu, L.; Li, P., The production of fully deacetylated chitosan by compression method. *The Egyptian Journal of Aquatic Research* **2016,** *42* (1), 75-81. DOI: 10.1016/j.ejar.2015.09.003

48. Wada, M.; Saito, Y., Lateral thermal expansion of chitin crystals. *J Polym Sci Pol Phys* **2001,** *39* (1), 168-174. DOI: 10.1002/1099-0488(20010101)39:1<168::Aid-Polb150>3.0.Co;2-0

49. Zhong, T. H.; Wolcott, M. P.; Liu, H.; Wang, J. W., Developing chitin nanocrystals for flexible packaging coatings. *Carbohydr. Polym.* **2019,** *226*. DOI: 10.1016/j.carbpol.2019.115276

50. Iwamoto, S.; Lee, S. H.; Endo, T., Relationship between aspect ratio and suspension viscosity of wood cellulose nanofibers. *Polym. J.* **2014,** *46* (1), 73-76. DOI: 10.1038/pj.2013.64

51. Satam, C. C.; Irvin, C. W.; Coffey, C. J.; Geran, R. K.; Ibarra-Rivera, R.; Shofner, M. L.; Meredith, J. C., Controlling Barrier and Mechanical Properties of Cellulose Nanocrystals by Blending with Chitin Nanofibers. *Biomacromolecules* **2020,** *21* (2), 545-555. DOI: 10.1021/acs.biomac.9b01268

52. Cao, H. C.; Thouless, M. D.; Evans, A. G., Residual-Stresses and Cracking in Brittle Solids Bonded with a Thin Ductile Layer. *Acta Metall.* **1988,** *36* (8), 2037-2046. DOI: 10.1016/0001-6160(88)90305-7

53. Fukuzumi, H.; Saito, T.; Isogai, A., Influence of TEMPO-oxidized cellulose nanofibril length on film properties. *Carbohydr. Polym.* **2013,** *93* (1), 172-177. DOI: 10.1016/j.carbpol.2012.04.069

54. Bigot, S.; Valentinčič, J.; Blatnik, O.; Junkar, M., Micro EDM parameters optimisation. In *4M 2006 - Second International Conference on Multi-Material Micro Manufacture*, Menz, W.; Dimov, S.; Fillon, B., Eds. Elsevier: Oxford, 2006; pp 195-198. DOI: 10.1016/B978-008045263-0/50045-3

55. Massey, L. K., Chapter 31 - Polyethylene Terephthalate (PET). In *Permeability Properties of Plastics and Elastomers (Second Edition)*, Massey, L. K., Ed. William Andrew Publishing: Norwich, NY, 2003; pp 189-199. DOI: 10.1016/B978-188420797-6.50033-4

56. Miller, K. S.; Krochta, J. M., Oxygen and aroma barrier properties of edible films: A review. *Trends Food Sci. Technol.* **1997,** *8* (7), 228-237. DOI: 10.1016/S0924-2244(97)01051-0

57. Choudalakis, G.; Gotsis, A. D., Permeability of polymer/clay nanocomposites: A review. *Eur. Polym. J.* **2009,** *45* (4), 967-984. DOI: 10.1016/j.eurpolymj.2009.01.027

58. Li, F.; Biagioni, P.; Bollani, M.; Maccagnan, A.; Piergiovanni, L., Multi-functional coating of cellulose nanocrystals for flexible packaging applications. *Cellulose* **2013,** *20* (5), 2491-2504. DOI: 10.1007/s10570-013-0015-3

59. Majoinen, J.; Kontturi, E.; Ikkala, O.; Gray, D. G., SEM imaging of chiral nematic films cast from cellulose nanocrystal suspensions. *Cellulose* **2012,** *19* (5), 1599-1605. DOI: 10.1007/s10570-012-9733-1

60. Gomez-Rios, D.; Barrera-Zapata, R.; Rios-Estepa, R., Comparison of process technologies for chitosan production from shrimp shell waste: A techno-economic approach using Aspen Plus (R). *Food Bioprod. Process.* **2017,** *103*, 49-57. DOI: 10.1016/j.fbp.2017.02.010

61. LCI summary for PLA and PET 12-ounce water bottles, 2007. Franklin Associates, Division of Eastern Research Group, Inc. http://www.petresin.org/pdf/FranklinPETPLAlifecycleanal_12-oz.pdf (accessed July 2021).

62. Park, S. H.; Lee, H. S.; Choi, J. H.; Jeong, C. M.; Sung, M. H.; Park, H. J., Improvements in barrier properties of poly(lactic acid) films coated with chitosan or chitosan/clay nanocomposite. *J. Appl. Polym. Sci.* **2012,** *125*, E675-E680. DOI: 10.1002/app.36405

63. Amjadi, S.; Emaminia, S.; Davudian, S. H.; Pourmohammad, S.; Hamishehkar, H.; Roufegarinejad, L., Preparation and characterization of gelatin-based nanocomposite containing chitosan nanofiber and ZnO nanoparticles. *Carbohydr. Polym.* **2019,** *216*, 376-384. DOI: 10.1016/j.carbpol.2019.03.062

64. Indumathi, M. P.; Sarojini, K. S.; Rajarajeswari, G. R., Antimicrobial and biodegradable chitosan/cellulose acetate phthalate/ZnO nano composite films with optimal oxygen permeability

and hydrophobicity for extending the shelf life of black grape fruits. *Int. J. Biol. Macromol.* **2019,** *132*, 1112-1120. DOI: 10.1016/j.ijbiomac.2019.03.171

65. Sharma, S.; Zhang, X. D.; Nair, S. S.; Ragauskas, A.; Zhu, J. Y.; Deng, Y. L., Thermally enhanced high performance cellulose nano fibril barrier membranes. *RSC Adv.* **2014,** *4* (85), 45136-45142. DOI: 10.1039/c4ra07469f

66. Nouri, A.; Yaraki, M. T.; Ghorbanpour, M.; Agarwal, S.; Gupta, V. K., Enhanced Antibacterial effect of chitosan film using Montmorillonite/CuO nanocomposite. *Int. J. Biol. Macromol.* **2018,** *109*, 1219-1231. DOI: 10.1016/j.ijbiomac.2017.11.119

TOC

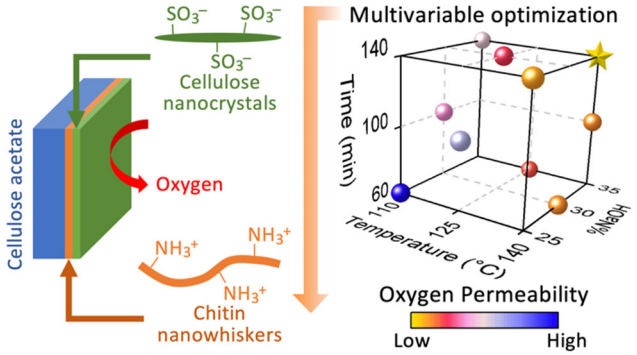

SYNOPSIS

Multilayer barrier films derived from biomass, including plants and food waste, have oxygen permeabilities comparable to petroleum-based materials for food packaging.